Theor Chim Acta (1988) 74: 123–135

Theoretica Chimica Acta

Tunnelling and reaction path curvature effects in the isomerization of the methoxy radical

Susan M. Colwell

University Chemical Laboratory, Lensfield Road, Cambridge, CB2 1EW, UK

(Received August 19/Accepted September 25, 1987)

The reaction path hamiltonian is used to investigate the isomerisation $CH_3O \rightarrow CH_2OH$; the reaction path, the frequencies along it and the coupling coefficients describing reaction path curvature were calculated by *ab-initio* methods. Correlation effects were included by configuration interaction using a double-zeta-plus-polarisation basis set. Including both tunnelling and curvature gives temperature dependent rate constants in broad agreement with experiment, whereas previous results were in error by several orders of magnitude.

Key words: Reaction path hamiltonian—Methoxy isomerization

1. Introduction

Now that *ab-initio* analytic gradient and second derivative calculations have become routine [1], it is becoming practical to investigate the dynamics of chemical reactions using accurate quantum chemical techniques. The reaction path hamiltonian (RPH) of Miller et al. [2] has made it feasable to use *ab-initio* methods to calculate reaction rates, and in particular, tunnelling contributions to these rates. The hamiltonian for a reacting system is expressed in terms of the reaction path, as defined by Fukui [3], and various quantities along it. The basic idea is to consider the potential as a one-dimensional barrier along the path and a multi-dimensional well in all perpendicular directions. Therefore it is not necessary to search large areas of the potential energy surface to define the hamiltonian. We have used the RPH to perform a detailed calculation on the contribution of tunnelling and reaction path curvature to the rate of isomerization

of the methoxy radical. This isomerization may be important for the oxidation of methoxy in the upper atmosphere. We presented some calculations on this system [4, 5] a few years ago, and have repeatedly been asked for the results of the more accurate calculations promised in that paper. The calculations described here use a higher level of quantum chemical theory, and give results in much better agreement with experiment than those previously described.

There have been many other calculations using the RPH and various authors have extended the theory [6–11] but we believe that this work is still the most complete treatment of a system of more than three atoms. We explicitly calculate the coupling coefficients that enable reaction path curvature to be taken into account, and we treat all of the 8 normal modes orthogonal to the reaction path, whereas most other authors ignore reaction path curvature and only consider one or two of the normal modes, treating the remainder as a heat bath.

1.1. The reaction path hamiltonian

The RPH of Miller et al. [2] has been described fully in earlier work, [6–8, 10, 11] and so is merely summarized here.

If $R_{i,\gamma} i = 1, \ldots, N$, $\gamma = x, y, z$ are the cartesian co-ordinates of an N atom system with a single saddle point separating reactants and products, and m_i, $i = 1, \ldots, N$ are the atomic masses, then the mass- weighted cartesian co-ordinates are $x_{i,\gamma} = m_i^{1/2} R_{i,\gamma}$. The reaction path, $\underset{\sim}{g}(s)$, is defined as "the path of steepest descent in mass-weighted cartesian co-ordinates from the saddle point to the products and to the reactants". i.e.

$$\underset{\sim}{g}'_{i,\gamma}(s) = -(\partial V/\partial x_{i,\gamma})/c^{1/2} \tag{1.1}$$

where $c = \sum_{i,\gamma} (\partial V/\partial x_{i,\gamma})^2$ is a normalization factor, and V is the potential energy as a function of the nuclear co-ordinates.

The reaction co-ordinate, s, is defined by

$$(ds)^2 = \sum_{i,\gamma} (dx_{i,\gamma})^2 \tag{1.2}$$

and gives the length along the reaction path. For zero total angular momentum, the hamiltonian can be written:

$$H(p_s, s; \underset{\sim}{P}, \underset{\sim}{Q}) = \frac{\frac{1}{2}\left[p_s - \sum_{k,k'=1}^{3N-7} Q_k P'_k, B_{kk'}, (s)\right]^2}{\left[1 + \sum_{k=1}^{3N-7} Q_k B_{k,3N-7}(s)\right]^2} + \sum_{k=1}^{3N-7} [1/2 P_k^2 + 1/2 \omega_k^2(s) Q_k^2] + V_0(s), \tag{1.3}$$

where: $Q_k, P_k, k = 1, \ldots, 3N\text{-}7$ are the normal co-ordinates and conjugate momenta for motion orthogonal to the reaction path, found from the $(3N\text{-}7)$ non-zero eigenvalues $\omega_k(s)$ and corresponding eigenvectors $[L_{i,\gamma,k}(s)]$ of the projected second derivative matrix at the point s.

The $\omega_k(s)$ give the frequencies of the transverse vibrations, $V_0(s)$ is the potential energy along the reaction path, and p_s is the momentum conjugate to s.

The $B_{k,k'}(s)$ which give the reaction path curvature are defined as follows

$$\text{(i)} \quad B_{k,k'}(s) = \sum_{i,\gamma} (\delta L_{i,\gamma,k}(s)/\delta s) L_{i,\gamma,k'}(s), \qquad k \neq k', \qquad k = 1, \ldots\ldots 3N\text{-}7 \tag{1.4}$$

are coriolis coupling coefficients which give the couplings of the normal modes with each other,

$$\text{(ii)} \quad B_{k,3N\text{-}6}(s) = \sum_{i,\gamma} (\delta L_{i,\gamma,k}(s)/\delta s) a'_{i,\gamma}(s), \qquad k = 1, \ldots\ldots 3N\text{-}7 \tag{1.5}$$

give the couplings of the vibrational modes to the reaction path, and

$$\text{(iii)} \quad B_{k,k}(s) = -\omega'_k(s)/(2\omega_k(s)) \tag{1.6}$$

are the diagonal elements.

Therefore, in order to define the reaction path hamiltonian for a given system, one needs to calculate:

(a) The stationary points, i.e. reactants, products, and transition state.

(b) The reaction path from the transition state to the reactants and to the products.

(c) The projected force constant matrix at various points along the reaction path, and its eigenvectors and eigenvalues, i.e. normal modes and frequencies. and,

(d) The coupling coefficients, $B_{k,k'}(s)$.

2. Stationary points

2.1. Equilibrium configurations

The equilibrium configurations of the ground states of CH_3O and CH_2OH were located using the Schlegel [12] and Murtagh Sargent optimization routines available in CADPAC [13]. These calculations were carried out using high spin open shell restricted hartree fock with a Dunning double zeta basis set [14]. The configurations found are given in Table 1.

Then the energy of each of these points was recalculated using singles + doubles configuration interaction (CI) with a Davidson correction, and a double zeta plus polarization basis set using p exponents of 1.0 on the hydrogens, and d exponents of 1.9 on the carbon and 1.2 on the oxygen. As shown in Table 1, the barrier height obtained was 37 kcal mol^{-1} and the endothermicity was -5 kcal-mol^{-1}, i.e. the reaction is exothermic.

This agrees well with other predictions: e.g. the most accurate calculations by Saebø et al. [15] give the barrier height to be at least 36 kcal mol^{-1} and the endothermicity to be -5 kcal/mol.

Haney and Franklin [16] conclude from thermochemical data that the reaction $CH_3O \rightarrow CH_2OH$ is exothermic by 5 ± 5 kcal mol^{-1}, and Wendt and Hunziker [17] obtained an exothermicity of 9 kcal/mol from heats of formation.

Table 1. Equilibrium configurations for methoxy, hydroxymethyl, and the transition state

	CH_3O	Transition state	CH_2OH
RCO/Å	1.434	1.416	1.391
RCH3/Å	1.084	1.295	1.991
RCH4/Å	1.081	1.074	1.070
RCH5/Å	1.081	1.074	1.077
ROH3/Å			0.951
OCH3	106.28	51.72	
OCH4	110.63	116.97	112.41
OCH5	110.63	116.97	117.94
H3OC			115.12
OCH3-H4	118.37	104.29	176.25
OCH3-H5	−118.37	−104.29	−37.29
H4CH5	110.87	119.46	120.14
RHF energy/hartree			
	−114.4034	−114.2913	−114.3875
CI energy/hartree			
	−114.7434	−114.6839	−114.7527
Barrier heights:	$E(TS)-E(CH_3O)=37.29$ kcal mol^{-1}		
	$E(TS)-E(CH_2OH)=43.15$ kcal mol^{-1}		
	$E(CH_3O)-E(CH_2OH)=-5.86$ kcal mol^{-1}		

Stationary points calculated to 10^{-6} in the gradients which imply 10^{-5} Å and 10^{-3} degrees for this basis set. See Fig. 1 for definition of labels

It would have been more accurate to optimize the geometry using CI with the larger basis set, but it would then have been necessary to calculate the frequencies along the reaction path by the same method, and this would have been unrealistically expensive. As the system is open shell, the quantum chemical calculations were not easy; severe convergence difficulties were met, as described in [4] and [5], and these increased with increasing level of calculation. It is well established for this type of molecule [18] that self consistent field (SCF) geometries calculated with a double zeta basis are much more accurate than the size of the basis set would suggest, and in fact are nearer to experiment than those calculated with a double zeta plus polarization basis. This is because the error due to the small size of the basis and the error caused by neglecting correlation cancel more effectively with this basis than with a larger one. It is also recognised that a singles plus doubles CI calculation with a double zeta plus polarization basis at these geometries will give a disproportionately accurate energy, and so this procedure seems justified.

3. Calculation of the reaction path

To start to locate the reaction path, it is necessary to identify the direction of negative curvature at the transition state. Therefore a second derivative calculation

was performed at the saddle point using the analytic second derivative method as implemented in CADPAC [13].

Once the direction of negative curvature has been identified, a small displacement δs is made along this line, and the energy and gradient calculated at the new point. The unit vector in the direction of the negative gradient vector is then calculated, and a small displacement is made along it. The energy and gradient are calculated at this new point, and the procedure is repeated until products or reactants are reached. All these calculations were done at the SCF level.

The reaction profile (i.e. energy versus reaction coordinate) was then scaled to give the CI barrier height and endothermicity. A different scaling factor was needed on each side of the barrier; the values used were: $\lambda_1 = 0.53$ (CH_3O to TS) and $\lambda_2 = 0.72$ (TS to CH_2OH). The reaction coordinate is unchanged by scaling. The scaled reaction profile is shown in Fig. 1.

The second derivative matrix was also calculated at each point on the reaction path as it was found. This matrix was then projected to remove motion along the reaction path as well as overall translational and rotational motion, and then diagonalised to give the harmonic frequencies $\omega_k(s)$ and the corresponding normal modes $L_{i,\gamma,k}(s)$. The vibrational frequencies calculated at CH_3O and

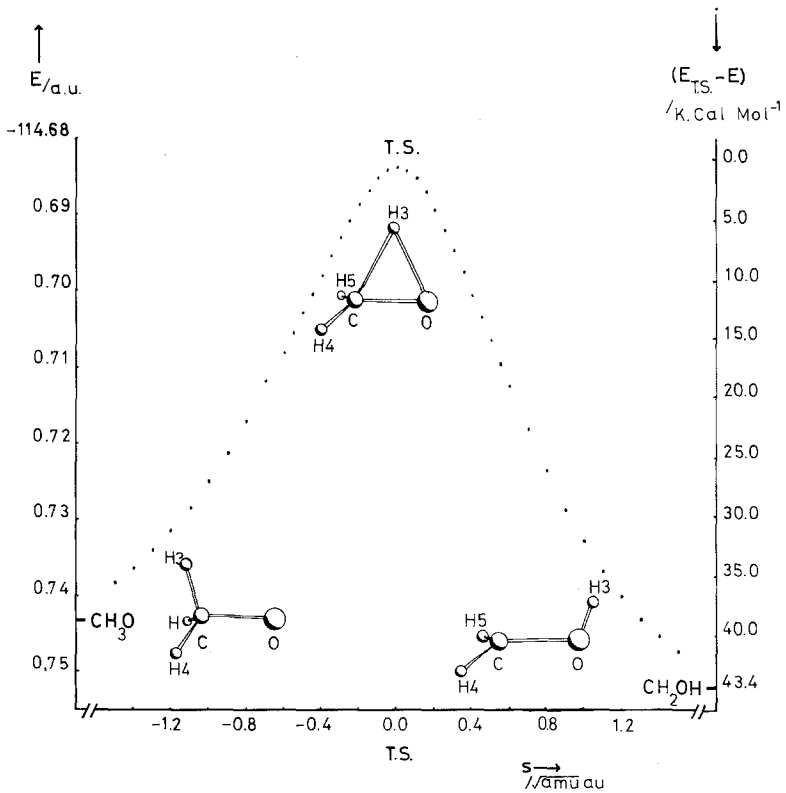

Fig. 1. Variation of scaled energy along the reaction path for the isomerization $CH_3O \rightarrow CH_2OH$

CH_2OH were then compared with experiment. A single linear scaling factor ($\lambda = 0.90$) was used which brought the calculated frequencies into closest agreement with experiment. This factor was used to scale all the frequencies at all points along the reaction path. The variation of scaled harmonic frequencies with reaction coordinate is shown in Fig. 2.

The modes are labelled as appropriate for the transition state. It at first appeared that there were two points at which the frequencies of two modes of the same symmetry appeared to cross (i.e. L_1 with L_4 at $s \approx -0.2$ and L_2 with L_3 at $s \approx -0.05$) but on more detailed examination it was found that the modes changed character along the path and were most appropriately identified in such a way that the crossings were avoided. The only frequencies that change appreciably are ω_6 and ω_1. L_6 looks like a CH stretch at CH_3O, a "ring breathing" at the saddle, and

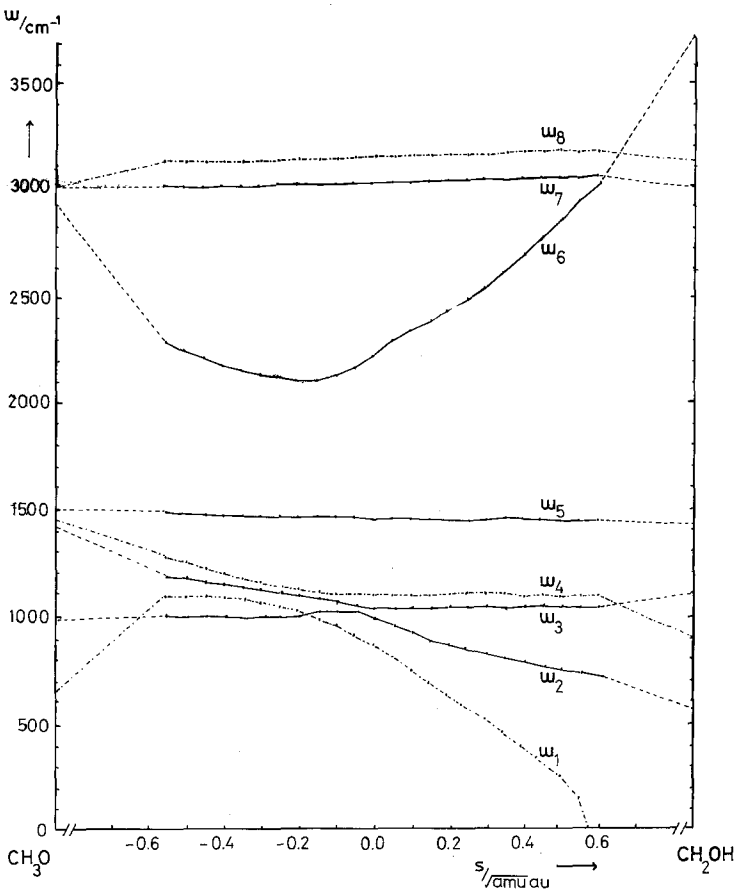

Fig. 2. Variation of the scaled projected harmonic frequencies along the reaction path for the isomerization $CH_3O \rightarrow CH_2OH$. The modes are labelled as appropriate for the transition state (TS). ω_1 torsion; $\omega_2 CH_2$ wag; $\omega_3 CO$ stretch; $\omega_4 CH_2$ Rock; ω_5 scissor; ω_6 ring breathing; ω_7 symmetric CH_2 stretch; ω_8 asymmetric CH_2 stretch

an OH stretch at CH_2OH, and so the frequency varies from a stretching to a bending and back to a stretching frequency during the reaction.

L_1 is the torsion mode, i.e. the out of plane motion of the odd hydrogen, and ω_1 decreases markedly as s increases towards CH_2OH. At $s=0.6$ ω_1 has become imaginary which implies that the second derivative matrix has a negative eigenvalue. Whilst all the ω_i^2 are positive the reaction path maintains the Cs symmetry of CH_3O and the transition state, but as CH_2OH has C_1 symmetry it is necessary for the symmetry to be broken at some point. The point at which ω_1 becomes zero ($s \approx 0.55$) is a bifurcation point, and there are then two equivalent reaction paths from this point, one to each of the two enantiomers of CH_2OH.

The points given in Fig. 1 for values of s larger than this, i.e. closer to CH_2OH, are therefore not on the true reaction path. There are two directions of negative curvature, and the system can be envisaged as moving along a ridge in the potential energy surface. This second negative curvature direction can be envisaged as a barrier for interconversion between the two equivalent forms of CH_2OH.

Clearly, beyond this bifurcation point, a simple picture of one-dimensional tunnelling is not appropriate. This point is, however, 7000 cm^{-1} below the top of the barrier, and as our previous calculations showed that this area of the potential curve is not important for tunnelling, no attempt was made to calculate the frequencies along the true reaction path past the bifurcation point.

4. Calculation of the coupling elements

The coupling elements $B_{k,k'}(s)$ involve the first derivatives of the normal modes w.r.t. distance along the reaction path. They cannot routinely be calculated analytically at present, as they involve energy derivatives of third order, and so must be calculated by finite difference techniques. As they have dimensions of (reaction coordinate)$^{-1}$ they are not affected by the scaling procedure. Details of the values of the $B_{k,k'}$ and the precise method of calculation can be found in paper [5]. As modes 1, 4 and 8 have a″ symmetry, their coupling with the reaction path and the other a′ modes is zero. As $B_{k,k'}(k \neq k')$ is skew symmetric, this further reduces the number of independent coriolis coupling coefficients from 56 to 13. There are also 5 non-zero $B_{k,F}$, and all 8 of the diagonal coupling elements, $B_{k,k'}$ must be used.

5. Calculation of reaction rates

5.1. The microcanonical rate constant $K(E)$

For the case $J=0$, the microcanonical rate constant is given by [19]

$$K(E) = N(E)/(2\pi\hbar\rho_0(E)) \tag{5.1}$$

where ρ_0 is the density of states at the reactants and $N(E)$ is the cumulative reaction probability. $\rho_0(E)$ is calculated from the classical Whitten-Rabinowitch

expression [20]

$$\rho_0(E) = E^{3N-7}/\left((3N\text{-}7)!\hbar^{3N-6}\prod_{i=1}^{3N-6}\omega_{i,0}\right). \tag{5.2}$$

5.2. The adiabatic approximation

The RPH given in (1.3) is most easily solved for the reaction probability using the vibrationally adiabatic approximation. This assumes that the motion along the reaction path is very slow compared with the transverse vibrations, and so all the normal modes stay in the same state during the course of the isomerization.

In terms of the action-angle variables for the transverse vibrational modes $(n_k + 1/2)$, q_k, $k = 1, \ldots, 3N\text{-}7$, the hamiltonian becomes:

$$H(p_s, s; \boldsymbol{n}, \boldsymbol{q}) = \sum_{k=1}^{3N-7}(n_k + 1/2)\omega_k(s) + V_0(s)$$
$$+ \frac{\frac{1}{2}\left[p_s - \sum_{k,k=1}^{3N-7}\left[((2n_k+1)(2n_{k'}+1)\omega_{k'}(s)/\omega_k(s))^{1/2}\cos q_{k'}\sin q_k B_{k,k'}(s)\right]\right]^2}{\left[1 + \sum_{k=1}^{3N-7}((2n_k+1)/\omega_k(s))^{1/2}\sin q_k B_{k,F}(s)\right]^2}. \tag{5.3}$$

If also the zero curvature approximation is used, the hamiltonian becomes:

$$H(p_s, s; \boldsymbol{n}) = \sum_{k=1}^{3N-7}(n_k + 1/2)\omega_k(s) + V_0(s) + 1/2p_s^2. \tag{5.4}$$

The n_k are constants of the motion for any fixed value of s, p_s, and by the adiabatic approximation they are constant as s changes. Therefore the motion can be regarded as being in the vibrational state $\boldsymbol{n}$ (n_i integers) perpendicular to the reaction path. The energy in each mode will change as $\omega_k(s)$ varies, but the n_k do not. The hamiltonian is thus reduced to that for the one dimensional problem of motion along the reaction path, which can be solved.

To apply the vibrationally adiabatic approximation to (5.3) retaining the curvature terms, it is necessary to regard s and p_s as paramters and to make a canonical transformation to the true action-angle variables of the system, $(N_k + 1/2)$, Q_k at each point. The hamiltonian will then be a function of $\boldsymbol{N}$, s, and p_s only, i.e. the N_i will be constants of motion for given s and p_s, and will stay constant as s and p_s vary, by the adiabatic approximation. Therefore, as in the zero curvature case, the system can be regarded as being in the vibrational state $\boldsymbol{N}$ (N_i integers) perpendicular to the reaction path, and the hamiltonian becomes essentially one-dimensional.

5.3. No tunnelling

Calculations were first performed without allowing for tunnelling. The reaction probability was taken to be:

$$1 \quad \text{if}(\boldsymbol{n} + 1/2) \cdot \boldsymbol{\omega} + V_{\max} < E \tag{5.5a}$$

and

$$0 \quad \text{if}(\boldsymbol{n}+1/2)\cdot\boldsymbol{\omega}+V_{\max}>E. \tag{5.5b}$$

For each value of E these probabilities were summed over all states $\boldsymbol{n}$, to give $N(E)$ and hence $K(E)$. Calculations were performed from the zero-point energy of CH_3O ($E_0=7921\ \text{cm}^{-1}$) to 26 000 cm^{-1} above it. The results are given in Fig. 3. $N(E)$ is zero until the classical threshold is reached ($E\text{-}E_0=11\,950\ \text{cm}^{-1}$) when one state ($\boldsymbol{n}=\mathbf{0}$) has enough energy in the reaction coordinate mode to overcome the barrier. At higher energies $N(E)$ involves the sum over typically 100 000 states (values of $\boldsymbol{n}$).

5.4. Vibrationally adiabatic zero curvature (VAZC)

The next approximation is to include the tunnelling but to assume zero curvature, which is equivalent to ignoring all the $B_{i,j}$ coupling elements. The hamiltonian is as given in (5.4) and can be rearranged to give:

$$p_s=\left(2\left[E-V_0(s)-\sum_{k=1}^{3N-7}(n_k+1/2)\omega_k(s)\right]\right)^{1/2}. \tag{5.6}$$

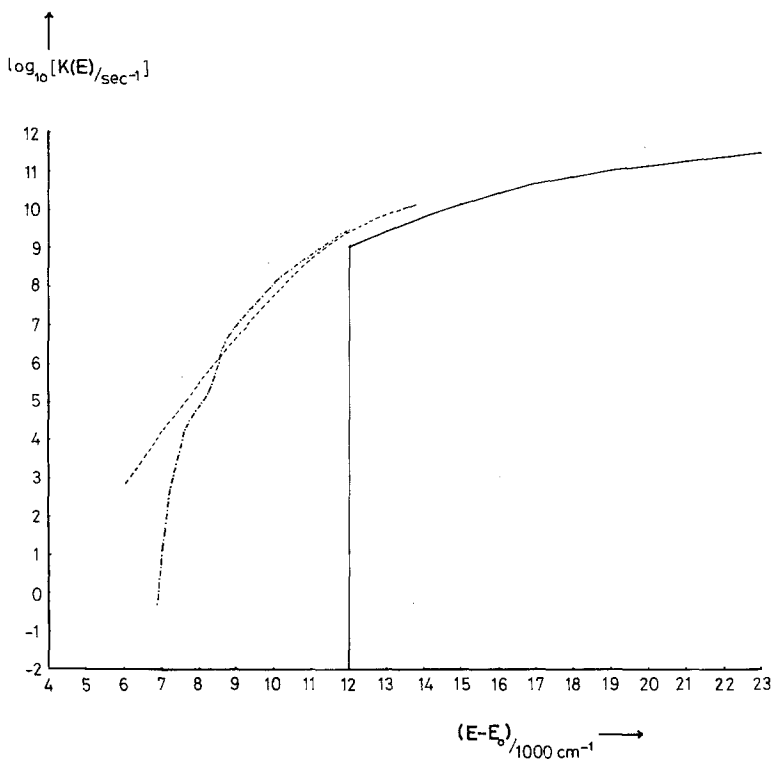

Fig. 3. Values of the microcanonical rate constant $K(E)$ for the reaction $CH_3O\rightarrow CH_2OH$. Zero point energy: $E_0=7921\ \text{cm}^{-1}$; classical threshold: $E-E_0=11\,953\ \text{cm}^{-1}$. Calculated (a) without tunnelling (——); (b) with tunnelling but without curvature (- - -), and (c) with both tunnelling and curvature (— · —)

Semiclassically, i.e. within the first order WKB approximation, $N(E)$ is given by:

$$N(E) = \sum_{n} [1 + \exp [2\theta(E, \boldsymbol{n})]]^{-1}, \tag{5.7}$$

where

$$\theta(E, \boldsymbol{n}) = \int_{s<}^{s>} ds \, \mathrm{Im} [p_s(s, E, \boldsymbol{n})] \tag{5.8}$$

is the barrier penetration integral, and $s>$ and $s<$ are the classical turning points. For each value of $\boldsymbol{n}$ (5.6) is solved for $p_s = 0$ to give $s<$ and $s>$, and $\mathrm{Im}(p_s)$ is integrated to give $\theta(E, \boldsymbol{n})$. The reaction probabilities are summed over all contributing states to give $N(E)$ and hence $K(E)$. States such that

$$E - V_{\max} - (\boldsymbol{n} + \mathbf{1/2}).\boldsymbol{\omega} < -6300 \text{ cm}^{-1} \tag{5.9}$$

were excluded from the calculation as they gave negligable reaction probabilities. At low energies only a few values of n contributed, at energies just below the classical threshold ≈ 1000 states contributed and at higher energies $N(E)$ involved the sum over $>100\,000$ states.

The results are shown in Fig. 3. $K(E)$ grows gradually from about 6000 cm^{-1} below the classical threshold. As would be expected, the VAZC results are always higher than the no-tunnelling ones, but this difference becomes less significant as the energy increases.

5.5. With curvature-theory

The simplest way to include curvature is to make the canonical transformation to the true action-angle variables of the system, $(N_i + 1/2, Q_i)$ at fixed s, p_s using 2nd order perturbation theory.

Assuming that the coupling elements, B, are small, and using Born's classical canonical perturbation theory [21], it can be shown that [5, 6]:

$$E_0(p_s, s; \boldsymbol{N}) = \tfrac{1}{2}p_s^2 + V(s; \boldsymbol{N}) + A(s; \boldsymbol{N}) + p_s^2 B(s; \boldsymbol{N}) - p_s^4 C(s) \tag{5.10}$$

where

$$V(s; \boldsymbol{N}) = V_0(s) + \sum_{k=1}^{3N-7} (N_k + 1/2)\omega_k(s). \tag{5.11}$$

and $A(s; \boldsymbol{N})$, $B(s; \boldsymbol{N})$ and $C(s)$ are algebraic expressions involving sums over rational functions of the B and the ω_i. The exact expressions are given in [5], Eqs. (5.24)-(5.26).

Therefore, using energy conservation, one has

$$-C(s)p_s^4 + (B(s; \boldsymbol{N}) + \tfrac{1}{2}p_s^2 + A(s; \boldsymbol{N}) + V(s; \boldsymbol{N}) = E \tag{5.12}$$

which can be solved to give:

$$p_s = (-2(V + A - E))^{1/2}[(B + \tfrac{1}{2} + ((B + \tfrac{1}{2})^2 + 4C(V + A + E))^{1/2}]^{-1/2}. \tag{5.13}$$

For a given choice of $\boldsymbol{N}$ (N_i integers) (5.13) can be solved for $p_s = 0$ to give the classical turning points. Im (p_s) can then be integrated between them to give $\theta(E, \boldsymbol{N})$ which can then be summed over all states $\boldsymbol{N}$ to give $N(E)$ and hence $K(E)$ as in the VAZC case.

5.6. With curvature-results

The results of these calculations are shown in Fig. 3. For energies 4000 cm^{-1} or more below the barrier, the microcanonical rate constants are reduced by curvature; for energies less than 4000 cm^{-1} below the barrier the rate constants are increased. As the energy increases, the two sets of results become almost identical. Because the effects of curvature are relatively small, it would appear that the use of perturbation theory is justified in this case.

5.7. Temperature dependent rate constants

The temperature dependent rate constant is given by [22]

$$K(E) = \left[\int_{E_0}^{\infty} N(E) \exp(-E/kT)\, dE\right] \Big/ \left[h \int_{E_0}^{\infty} \omega_0(E) \exp(-E/kT)\, dE\right] \tag{5.14}$$

where E_0 is the zero-point energy of the reactant. This can be written in the lagnuage of transition state theory (TST) as:

$$K(T) = kT/h \frac{z\ddagger}{z} \tag{5.15}$$

with

$$Z\ddagger = \int_{E_0}^{\infty} N(E) \exp(-E/kT) d(E/kT) \tag{5.16}$$

$$Z = \int_{E_0}^{\infty} \rho_0(E) \exp(-E/kT)\, dE. \tag{5.17}$$

This differs from the usual TST expression as the integral for Z^+ extends down to E_0 to take into account the tunnelling contribution from all the reactant energies. The expression for $N(E)$ involves the values of $V(s)$, the variable frequencies $\omega_k(s)$, and the curvature elements $B_{k,k'}(s)$ for a range of values of s along the reaction path, not just their values at the transition state. In the no-tunnelling case this does reduce to the usual TST expression.

Equation (5.17) was integrated numerically to give $K(T)$ for values of T between 100 K and 1000 K. The results are shown in Table 2.

It can be seen that the rate constants calculated with tunnelling (Cols 2 and 3) are significantly higher than those calculated without (Col 1), therefore showing the importance of including tunnelling in these investigations. As with the microcanonical rates, the effects of including curvature are not uniform; below 450K

Table 2. Temperature dependent rate constants for the isomerization of the methoxy radical

$K(T)/s^{-1}$ /K	No tunnelling	With tunnelling VAZC[a]	With curvature[b]
100	0	0.22×10^{-32}	0.15×10^{-39}
200	0.11×10^{-24}	0.17×10^{-13}	0.20×10^{-16}
300	0.34×10^{-12}	0.55×10^{-7}	0.43×10^{-8}
400	0.61×10^{-6}	0.23×10^{-3}	0.15×10^{-3}
500	0.36×10^{-2}	0.93×10^{-1}	0.12×10^{0}
600	0.12×10^{1}	0.97×10^{1}	0.13×10^{2}
700	0.83×10^{2}	0.36×10^{3}	$0.43\times10^{+3}$
800	0.20×10^{4}	0.63×10^{4}	0.69×10^{4}
900	0.25×10^{5}	0.62×10^{5}	0.65×10^{5}
1000	0.19×10^{6}	0.41×10^{6}	0.42×10^{6}

[a] Vibrationally adiabatic zero curvature approximation. See Sect. 5.4
[b] With curvature. See Sect. 5.5

curvature decreases the rate constant, above 450K the rates are increased. For example at 700K the rate is increased from 0.36×10^{3} to 0.43×10^{3} per second, but at 1000K the corresponding rates are 0.41×10^{6} and 0.42×10^{6} per second.

These results are in broad agreement with the values estimated from thermochemical considerations by Batt et al. [23], who give upper bounds of $10^{-6}\,s^{-1}$ at 300 K and $2\times10^{4}\,s^{-1}$ at 650 K. Our previous results differed from these by about ten orders of magnitude, and so were not chemically useful. This present work demonstrates that it is essential to include correlation effects, and that when they are included it is possible to get reaction rates which are chemically meaningful.

6. Summary

In this paper a very detailed quantum mechanical calculation has been performed for the isomerization $CH_3O \rightarrow CH_2OH$. The reaction path has been found, and frequencies and normal co-ordinates orthogonal to the path have been determined. The theory of the reaction path hamiltonian has been used to calculate the microcanonical and temperature-dependent rate constants using a semiclassical perturbation theory approach including both the effects of tunnelling and reaction path curvature.

Although this calculation was computationally rather expensive, and the procedure is in no sense automatic, it does demonstrate the power path hamiltonian methods to give chemically reasonable answers for quite large systems.

References

1. For a review see: Pulay P (1987) In: Lawley KP (ed) *Ab initio* methods in quantum chemistry, part II (Advances in chemical Physics, vol LXIX, pp 41–286) Wiley, New York
2. Miller WH, Handy NC, Adams JE (1980) J Chem Phys 72:99

3. Fukui K (1970) J Phys Chem 74:4161
4. Colwell SM (1984) Mol Phys 51:1217
5. Colwell SM, Handy NC (1985) J Chem Phys 82:1281
6. Gray SK, Miller WH, Yamaguchi Y, Schaefer HF (1980) J Chem Phys 73:2733
7. Waite BA, Gray SK, Miller WH (1983) J Chem Phys 78:259
8. Miller WH (1983) J Phys Chem 87:3811
9. Tachibana A, Okazaki I, Koizumi M, Hori K, Yamabe T (1985) J Am Chem Soc 107:1190
10. Miller WH (1986) In: Clary DC (ed) The theory of chemical reaction dynamics. Reidel, Dordrecht
11. Truhlar DG, Brown, FB, Steckler R, Isaacson AD (1986) In: Clary DC (ed) The theory of chemical reaction dynamics. Reidel, Dordrecht
12. Schlegel B (1982) J Comput Chem 3:214
13. Amos RD (1984) CADPAC, the Cambridge analytical derivatives package. CCP1/8414 SERC Daresbury Laboratory, Daresbury, Warrington
14. Dunning TH (1970) J Chem Phys 53:2823
15. Saebø S, Radom L, Schaefer HF (1983) J Chem Phys 78:845
16. Haney MA, Franklin JL (1969) Trans Faraday Soc 65:1974
17. Wendt HR, Hunziker HE (1979) J Chem Phys 71:5202
18. Hehre WJ, Radom L, Schleyer PVR, Pople JA (1986) *Ab initio* molecular orbital theory, chap 6.2. Wiley New York
19. Miller WH (1979) J Am Chem Soc 101:6810
20. E.g., Robinson PJ, Holbrook KA (1972) Unimolecular reactions. Wiley, New York
21. Born M (1960) The mechanics of the atom. Ungar, New York
22. Miller WH (1982) J Chem Phys 76:4904
23. Batt L, Burrows JP, Robinson GN (1981) Chem Phys Lett 78:467